TECHNICAL ARTICLE

20 GHz Direct Sampling: All in One Nyquist—Part 2: Quadrature Interleaving

Ian Beavers, Field Applications Engineer,
Peter Delos, Senior Principal Engineer,
Brian Reggiannini, Senior Principal Engineer, and
Connor Bryant, System Applications Engineer

Abstract

Direct RF sampled systems are evolving to encompass broader capabilities, allowing them to capture a wider bandwidth all in a single Nyquist zone. Sampling from 2 GHz to 18 GHz concurrently enables more sophisticated options to monitor a larger spectrum, without issues of frequency band aliasing. Quadrature interleaving offers a novel solution to expand sampling bandwidth without the complexities of managing double rate clocks, clock inversion, or doubling the data output.

Introduction

Part 1 describes the interleaving objectives, discusses errors creating interleaving artifacts, and introduces the range of 40 GSPS analog-to-digital converter (ADC) options using the AD9084. Part 2 explores the quadrature sampling option, along with a quadrature correction mechanism in detail.

An emerging capability that is enhancing data converter products is the significant inclusion of embedded digital signal processor (DSP) cores. A relevant example of showcasing embedded DSP included in modern ADCs is to double the effective sample rate without increasing the back-end digital data rates. Using two ADCs with quadrature inputs and a quadrature correction algorithm, a dual 40 GSPS ADC can be configured to produce four 4 GHz digitally downconverted outputs, monitoring a 2 GHz to 18 GHz bandwidth, within a single multichannel converter IC.

First, direct quadrature sampling is described relative to the more common zero IF (ZIF) architectures. Quadrature errors are acknowledged, along with a description of the embedded digital processing needed for quadrature error correction (QEC). Analog RF front-end components, sampling of ADC data, embedded DSP processing, and final processing of data converter I/Q outputs are used. The measured results show amplitude and phase errors both before and after QEC, and the final measured image rejection demonstrates effective direct quadrature sampling from 2 GHz to 18 GHz. The approach is described for the AD9084 IC, yet is generally extendable to any wideband sampling system.

Quadrature Sampling Principles

A traditional ZIF architecture is shown in Figure 1.[1] The architecture creates two IF signals in quadrature (90° out of phase) through a quadrature RF downconverting mixer. In this case, the quadrature is created in the local oscillator (LO) circuitry from two sets of physically separated mixers and LOs, each 90° out of phase. The result is two IF frequencies in quadrature. The ability to resolve whether the RF is above or below the LO frequency is visualized by a phase reversal between the I and Q signals at the LO frequency, as shown in Figure 1. Digital downconverters (DDCs) processing real data converter data streams and creating an I/Q output data stream at a reduced bandwidth centered by a numerically controlled oscillator (NCO) are also enabled by these same principles.

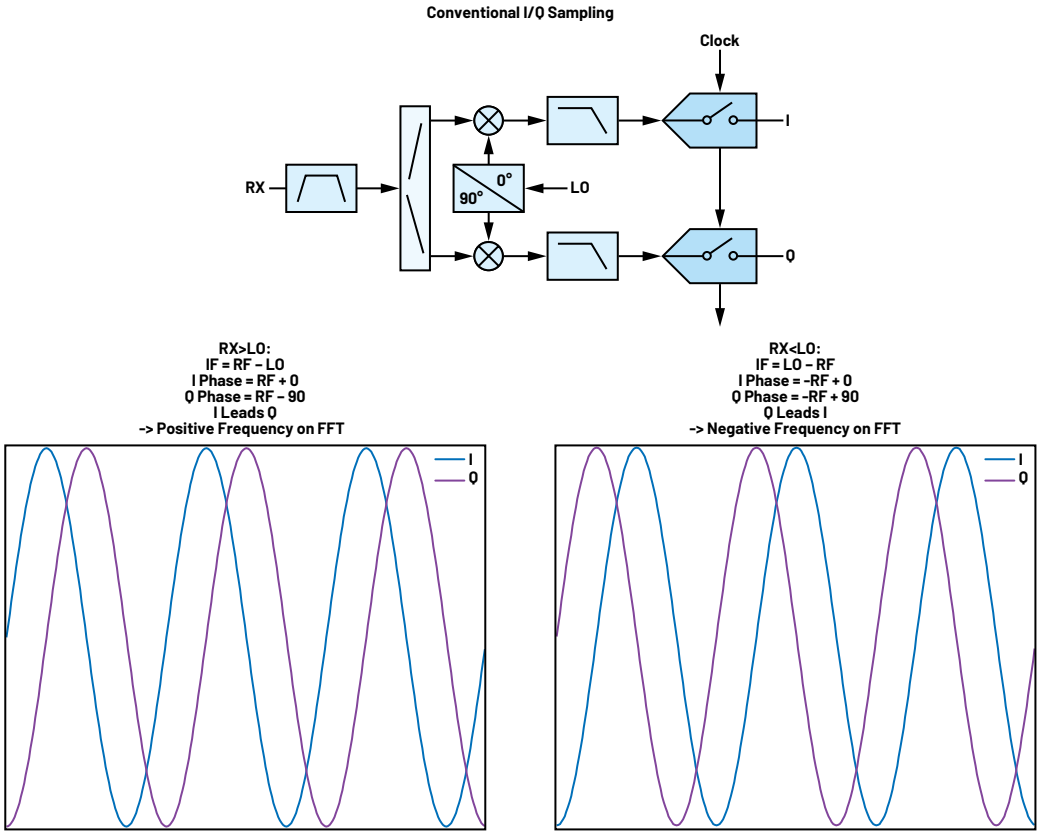

Figure 1. Quadrature sampling principles compared with a ZIF architecture.

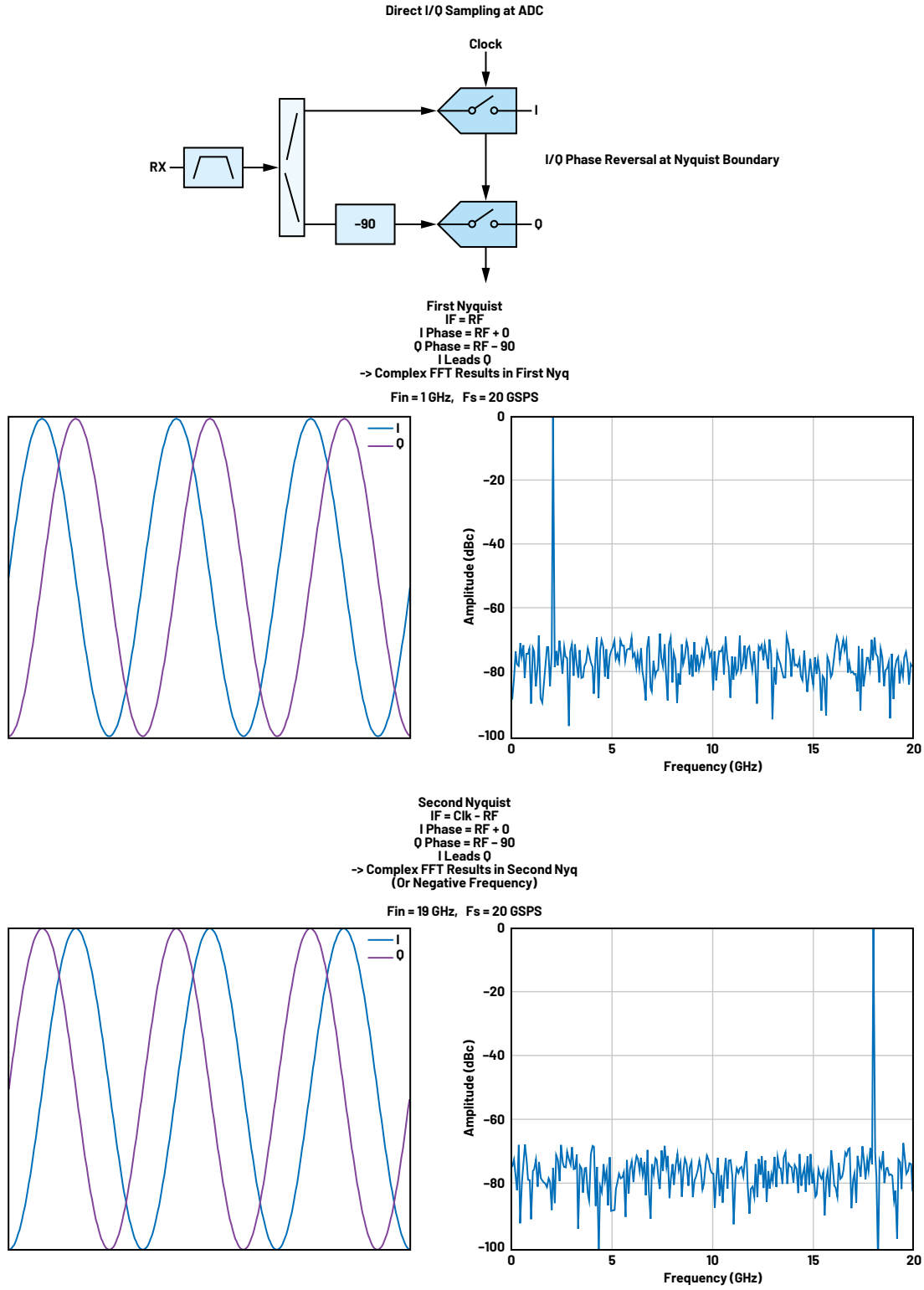

Figure 1 (continued). Quadrature sampling principles compared with a ZIF architecture.

The principles in Figure 1 enable the description of direct quadrature sampling. If the 90° phase shift is moved such that two parallel ADCs simultaneously sample the same RF input placed in quadrature, there is a phase reversal of the I/Q signals at the Nyquist boundary through the sampling process. This property can be exploited to effectively double the ADC sample rate and is shown in Figure 2.

In practice, the 90° phase shift is accomplished with a hybrid coupler, also marketed as a hybrid splitter. Wideband hybrid couplers are now available covering a 2 GHz to 18 GHz bandwidth.

Quadrature Errors

A well-known issue in quadrature sampling is any phase or amplitude mismatch in the I/Q balance creates unwanted perceived energy at the image frequency. This issue also applies to the direct quadrature sampling approach and needs to be addressed with a back-end algorithm.[2] The operational concern is shown in Figure 2. The concern is that an unwanted signal in the image band can fold back into the signal band. The level of the image is a function of the amplitude and phase mismatch from the ideal quadrature and creates the need for a QEC method.

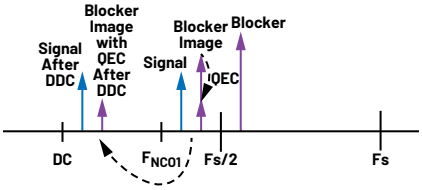

Figure 2. Direct quadrature sampling image: The concern in direct quadrature sampling is that an unwanted signal in the image band can fold to the signal band. The level of the image is a function of the amplitude and phase mismatch from the ideal quadrature and is seen in the blocker image level compared to the blocker level. The blocker image is further reduced with a QEC method.

Image rejection levels can be calculated as follows:

IRR = Image Reject Ratio (dB)

$P = 10^{(IRR/10)}$

A = Amplitude Mismatch

θ = *Phase Error*

For a given IRR and amplitude error

$$\theta = acos\left(-\frac{(1+A^2)(P-1)}{2A(P+1)}\right) \quad (1)$$

For a given IRR and phase error

$$a = P - 1 \quad (2)$$

$$b = 2(P+1)\cos\theta \quad (3)$$

$$A = \frac{-b \pm \sqrt{b^2 - 4a^2}}{2a} \quad (4)$$

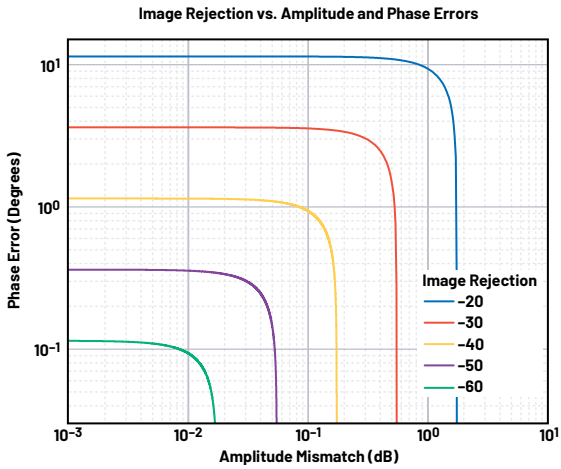

Figure 3. Amplitude and phase errors between the I and Q channels to achieve specific image rejection values. Axes are shown on a log-log scale.

Figure 3 plots the image rejection magnitude vs. the required amplitude and phase error. As an example, a 60 dBc image rejection magnitude requires a phase accuracy of less than one-tenth of a degree and an amplitude match to within hundredths of a dB. This level of image rejection is not practical in hardware alone using the accuracy of currently available commercial RF components. Therefore, to utilize the direct quadrature sampling approach, additional digital error correction is needed. The configurations used for QEC will be described in the following sections.

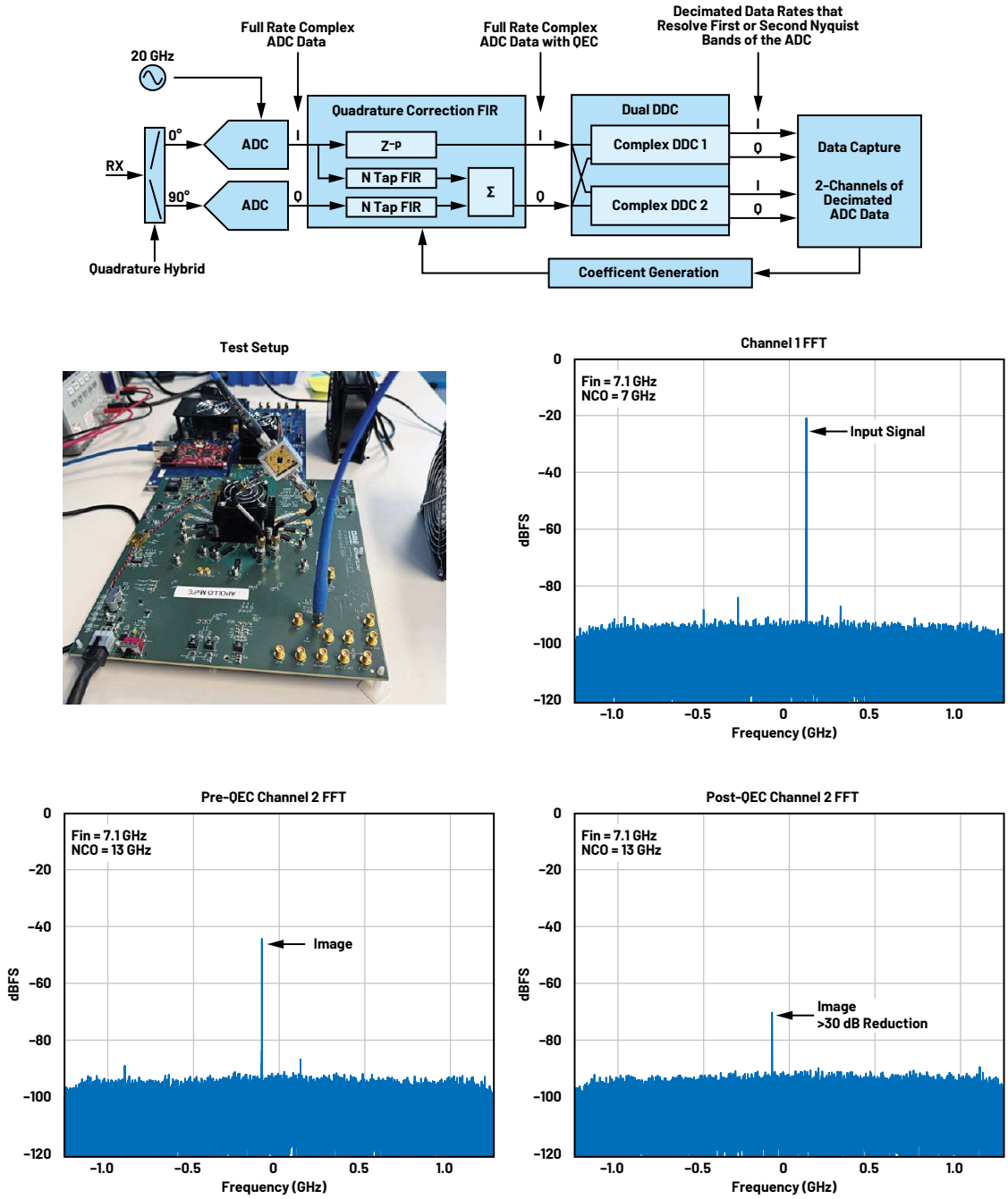

Figure 4. The AD9084 direct quadrature sampling configuration using the PFILT in a half-complex finite impulse response (FIR) filter mode for QEC.

Quadrature Sampling with Programmable Filter (PFILT) QEC

A block diagram of the AD9084 configuration for direct quadrature sampling with PFILT QEC is shown in Figure 4. For the measured FFTs shown, the input frequency was set to 7.1 GHz, the NCO in Channel 1 was set to 7 GHz, and the input signal appeared in the baseband data at 100 MHz. The image frequency is mirrored around $f_s/2$ and appears at 12.9 GHz. The channel 2 NCO was set to 13 GHz to monitor the image frequency that appears in the baseband output at –100 MHz.

The sequence of steps for test data in subsequent figures is as follows:

A functional verification is performed, then the background ADC calibrations are frozen to prevent deviations across channels due to further ADC calibrations. Next, the frequency was swept in 25 MHz steps across a 4 GHz BW. For each data capture, the NCO1 frequency was set to Fin – 100 MHz and for the second NCO, NCO2, the frequency was set to 20 GHz – NCO1 frequency. This results in both NCO frequencies mirroring the sample rate divided by two, $f_s/2$.

Based on measured Ch1 and Ch2 data, quadrature correction coefficients are then calculated and applied to the embedded FIR as seen in Figure 5. Additional data was retaken and the post QEC performance was then evaluated. This sequence was repeated four times to cover the full 2 GHz to 18 GHz operating range.

The result of 4 GHz bandwidth corrections is shown below. The AD9084 has four banks of filter coefficients that can be rapidly selected. This programmable feature allows the used coefficients to be optimized based on the input frequency of interest based, given the programmed NCO frequency.

The suitability of the half-complex PFILT structure can be illustrated with a simple example. The direct quadrature sampling configuration involves splitting the signal into separate I and Q paths that are each sampled by individual ADCs.

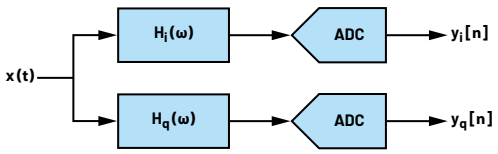

Figure 5. Quadrature sampling mode.

QEC is a relative form of equalization. For example, the I path can be thought of as ideal, and the Q path can be matched to the I path. Therefore, the response of the Q path can be modeled as the combination of (a) a nominal 90° phase shift, (b) the common response of the I path, and (c) a mismatch or delta response of the Q path relative to the I path as shown in Figure 6.

$$H_i(\omega) = 1 \tag{5}$$

$$H_q(\omega) = H_{90}(\omega)H_i(\omega)H_\Delta(\omega) \tag{6}$$

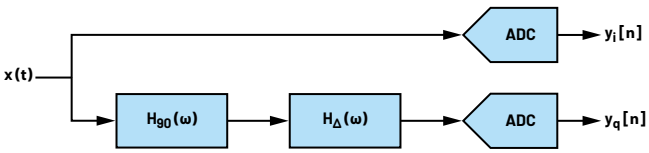

Figure 6. Relative quadrature sampling model in terms of nominal 90° phase shift $H_{90}(\omega)$ and Q vs. I mismatch response $H_\Delta(\omega)$.

Figure 7 shows the result of stimulating this relative quadrature sampling model with a sinusoidal input $x(t) = \cos(\omega_0 t)$. The nominal 90° phase shift converts a cosine to a sine, and the delta response $H_\Delta(\omega) = A_\Delta(\omega)e^{(j\theta_\Delta(\omega))}$ modifies the amplitude and phase of the result.

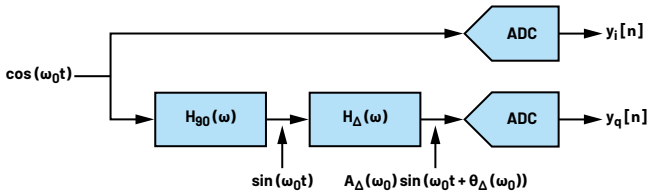

Figure 7. Stimulating the quadrature sampling model with a cosine input results in a sine input to the second ADC along with the amplitude and phase errors.

Using a simple trigonometric identity, the output of the Q path can be decomposed into sine and cosine parts.

$$y_i(t) = \cos(\omega_0 t) \tag{7}$$

$$y_q(t) = A_\Delta(\omega_0)\cos(\theta_\Delta(\omega_0))\sin(\omega_0 t) + A_\Delta(\omega_0)\sin(\theta_\Delta(\omega_0))\cos(\omega_0 t) \tag{8}$$

In the absence of a mismatch between the I and Q paths ($H_\Delta(\omega) = 1$), the ideal outputs of the quadrature sampling configuration can be defined as:

$$x_i(t) = \cos(\omega_0 t) \tag{9}$$

$$x_q(t) = \sin(\omega_0 t) \tag{10}$$

Therefore, for a sinusoidal or other narrowband signal centered at frequency ω_0, the actual quadrature outputs can be written in terms of the ideal quadrature outputs. The direct quadrature configuration can be viewed as a 2 × 2 linear system that generates quadrature error. QEC is performed by inverting this 2 × 2 linear system to recover the ideal outputs $x_i(t)$ and $x_q(t)$.

$$y_i(t) = x_i(t) \tag{11}$$

$$y_q(t) = A_\Delta(\omega_0)\cos(\theta_\Delta(\omega_0))\,x_q(t) + A_\Delta(\omega_0)\sin(\theta_\Delta(\omega_0))\,x_i(t) \tag{12}$$

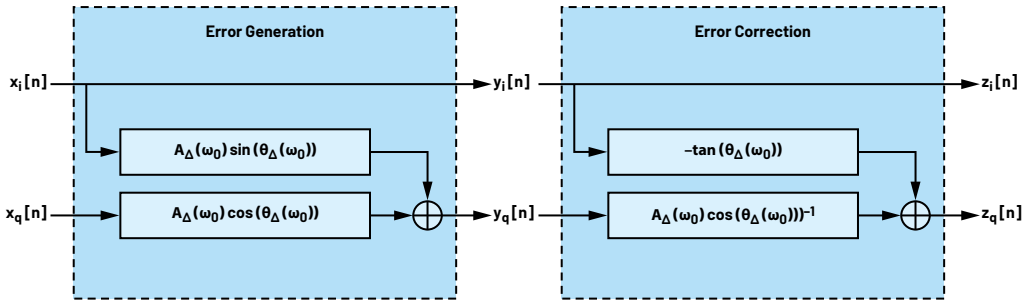

Figure 8. A quadrature sampling model extended to show both the error terms and the error correction. The topology shown is a half-complex filter and is consistent with the filter shown in Figure 4.

The analysis in Figure 8 describes the generation and correction of quadrature error when the system is stimulated at a single frequency. Because the 2 × 2 system is linear, the solution is easily generalized to wideband signals by introducing multitap FIR filters that vary their amplitude and phase responses over frequency.

Quadrature Sampling with CFIR QEC

The PFILT runs at the full 20 GSPS sample rate behind each ADC. The AD9084 also includes a complex FIR (CFIR) after the decimation. The benefit of using this filter is that the correction can be applied over a longer time without increasing the number of filter taps. To accomplish this, both complex DDCs (CDDCs) are used. The second CDDC shifts the image frequency to be the negative frequency of the image within the primary DDC. By summing a weighted version of the complex conjugate of the second CDDC, an image cancellation is created. The approach is shown in Figure 9.

The CFIR performs QEC in the same way that the PFILT does. The only difference is that the correction is applied to the decimated output. To show that this is the case, the PFILT can be viewed as a network of complex filters, as opposed to the 2 × 2 linear system that was previously described. The 2 × 2 linear system has the form shown below, where the inputs, outputs, and filter coefficients are all real-valued, and the * symbol indicates convolution.

$$z_i[n] = y_i[n] \tag{13}$$

$$z_q[n] = a_i[n] * y_i[n] + a_q[n] * y_q[n] \tag{14}$$

If these real-valued signals are combined and interpreted as complex-valued signals, then the following properties hold true.

$$y[n] = y_i[n] + jy_q[n] \tag{15}$$

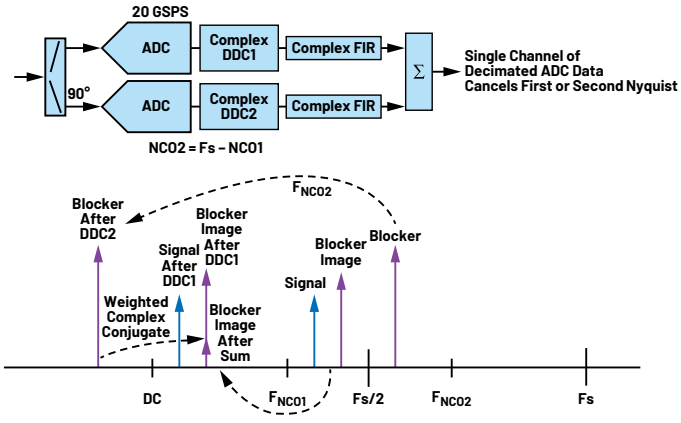

Figure 9. Direct quadrature sampling with CFIR QEC.

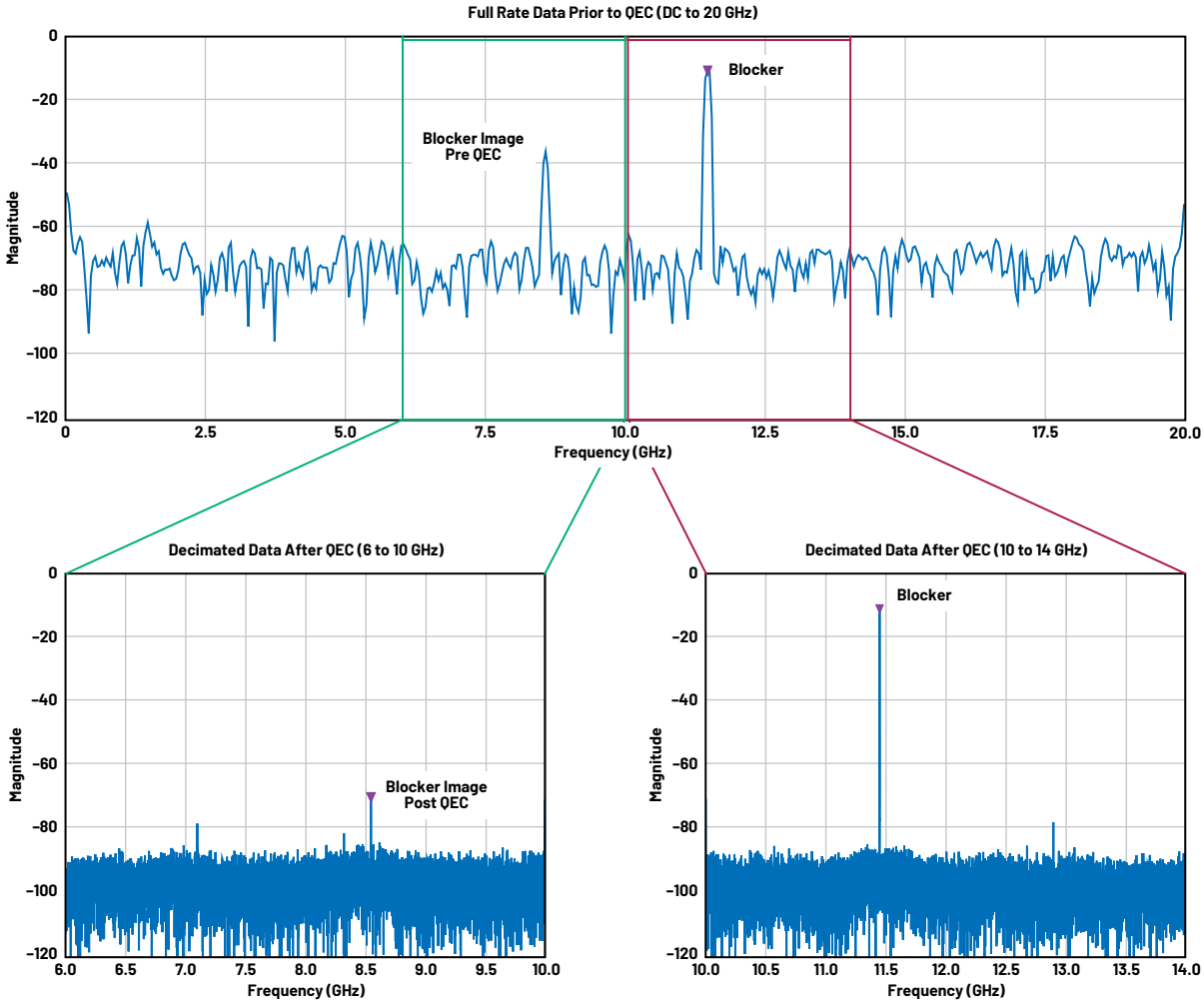

Figure 10. Representative quadrature sampling FFT measurements using the CFIR for QEC. A blocker is injected at 13 GHz creating an image at 7 GHz. The upper plot is a full rate data capture of a 40 GSPS FFT before QEC. The lower plots are FFTs of decimated data showing the blocker image was reduced below 60 dBc.

$$y_i[n] = \frac{1}{2}\left(y[n] + y^*[n]\right) \tag{16}$$

$$y_q[n] = \frac{1}{2j}\left(y[n] - y^*[n]\right) \tag{17}$$

By defining $y[n] = y_i[n] + jy_q[n]$ and substituting via the properties given above, the complex-valued interpretation of the half-complex PFILT structure can be derived.

$$z[n] = (b_1[n] * y[n]) + (b_2[n] * y[n])^* \tag{18}$$

$$b_1[n] = \frac{1}{2}\left(\delta[n] + ja_i[n] + a_q[n]\right) \tag{19}$$

$$b_2[n] = \frac{1}{2}\left(\delta[n] + ja_i[n] - a_q[n]\right) \tag{20}$$

The result is an alternative interpretation of the effect of the PFILT that involves:

1. Applying a complex-valued linear filter $b_1[n]$ to the complex-valued input $y[n]$. Filter $b_1[n]$ performs an in-band equalization of Q compared to I in order to preserve the flatness of the desired signal.
2. Applying a complex-valued linear filter $b_2[n]$ to the complex-valued input $y[n]$. Filter $b_2[n]$ transforms the blocker signal into an anti-image that will sum destructively with the unwanted image.
3. Summing the output of the first filter with the complex conjugate of the output of the second filter. Conjugation in time causes a flip in frequency that aligns the blocker and its image in frequency, allowing a scaled and rotated version of the blocker to sum destructively with its image.

These are the exact steps performed by the DDCs and CFIRs to achieve QEC.

1. DDC1 downconverts the desired signal, and CFIR1 applies a complex-valued linear filter with response equivalent to $b_1[n]$ (but shifted in frequency and applied at a lower sampling rate).
2. DDC2 downconverts the blocker signal, and CFIR2 applies a complex-valued linear filter with response equivalent to $b_2[n]$ (but shifted in frequency and applied at a lower sampling rate).
3. Summing the outputs of CFIR1 and CFIR2 results in the image rejection.

Example FFT measurements using the CFIR to achieve QEC are shown in Figure 10.

Quadrature Error Training Approach

The Quadrature Sampling with Programmable Filter section explains that discrepancies between the I and Q paths lead to quadrature errors. It also details how, if these mismatches were identified, the errors could be rectified using the half-complex PFILT structure. The Quadrature Sampling with CFIR QEC section proves that the same QEC can also be deferred to the CFIRs at the outputs of the DDCs. In both cases, the coefficients of the ideal correction filters depend on the mismatch response between the I and Q paths. This section describes one way that the mismatch response can be estimated.

Multiple types of QEC algorithms exist. One way of differentiating between algorithms is based on the input stimulus used for training.

- Online calibrations are conducted while the system remains active, normally training opportunistically using whatever input signal is presented to the ADC. These calibrations can run in the background for extended periods and can adapt to changes in I/Q mismatch due to drifts in temperature, supply, and timing.
- Offline calibrations function when the system is not active. Because the system is offline, known calibration signals can be injected for training purposes. Once training is completed, the system can be brought back online, operating with fixed correction coefficients. Depending on the use case, the system might require periodic recalibration as system parameters drift. The system must be brought offline again during recalibration.

The choice of online or offline calibration is application specific, as there are pros and cons to both approaches. The remainder of this discussion focuses on a form of offline calibration that injects a series of calibration tones into the system.

This calibration defines two bands of interest as shown in Figure 11.

- The desired band covers the desired output bandwidth of the system.
- The blocker band is mirrored across $f_s/2$ relative to the desired band, where f_s is the ADC sampling rate. For example, if the desired band spans from frequency f1 to frequency f2, then the blocker band spans from f_s - f2 to f_s - f1. Large blocking signals that appear within the blocker band will generate a false image that falls within the desired band.

These two bands of interest can span anywhere within DC to $f_s/2$ and can overlap.

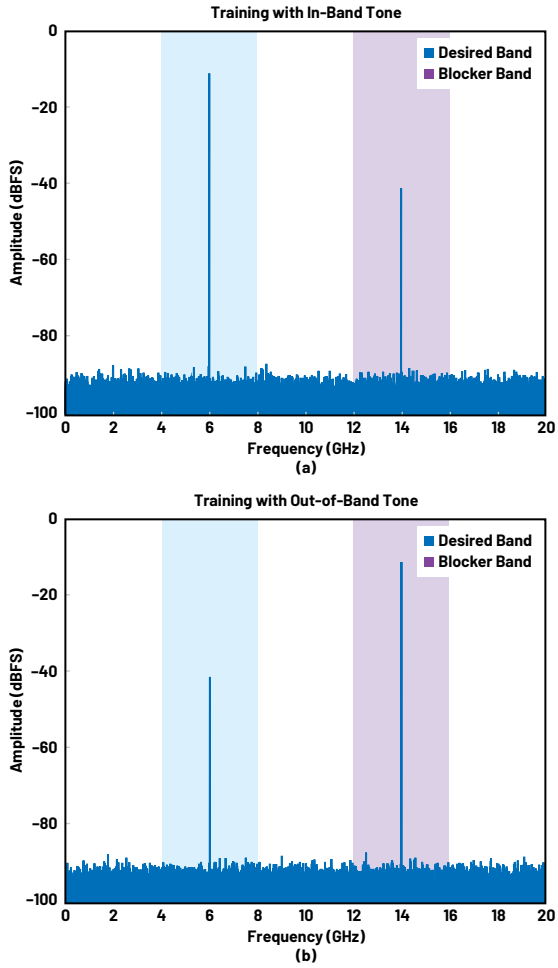

Figure 11. QEC training involves sweeping frequencies both within the band of interest to ensure amplitude flatness and within the image band to ensure image rejection.

With respect to these two bands of interest, the QEC calibration has two objectives.

1. Reject images that fall within the desired band.
2. Preserve signals that fall within the desired band by matching the in-band gain and phase response of the Q path to the in-band gain and phase response of the I path. This is a relative form of equalization. The Q path is matched to the I path, but any droop within the I path is preserved.

These two objectives are related through I/Q mismatch. As the Q path is matched to the I path, both in-band flatness and out-of-band image rejection are improved simultaneously. Therefore, to achieve both objectives, the calibration must learn the I/Q

mismatch for both the desired band and the blocker band, and then tune the coefficients of the correction filter to perform relative Q-to-I equalization across both bands.

However, the two objectives are not necessarily weighted equally. For many applications, from an I/Q matching perspective, in-band flatness requirements can be met with a relatively coarse I/Q matching, while image rejection targets typically require much more accurate I/Q matching.

Table 1 shows the in-band gain and phase errors corresponding to various levels of image rejection. For example, if an application requires 1° in-band flatness and –50 dBc image rejection, the I/Q matching required to achieve the image rejection target is approximately five times more precise than what is needed for in-band flatness.

Table 1. Minimum Errors Required for Image Rejection Performance

Image Rejection (dBc)	In-Band Gain Error (dB)	In-Band Phase Error (deg)
–20	0.9151	5.7106
–30	0.2791	1.8112
–40	0.0873	0.5729
–50	0.0275	0.1812
–60	0.0087	0.0573

Table 2 shows an example training algorithm that applies an unequal weighting for the flatness compared to the image rejection objectives. Calibration tones are injected within the desired band so that in-band flatness can be improved within the desired band. Calibration tones are injected within the blocker band so that images that fall within the desired band can be attenuated. When the desired band spans across $f_s/2$, then the desired band and the blocker band overlap. Calibration tones that fall within the overlap region can be labeled as if they fall within the blocker band, thus giving them a larger weighting factor to achieve the more difficult image rejection objective.

Table 2. Training Algorithm

Offline Tone-Based QEC calibration			
	Define a set of tone frequencies f_k for $k = 1,\ldots,K$ that span the union of the desired band and the blocker band.		
	Define a weighting factor λ_{in} for in-band flatness objective.		
	Define a weighting factor λ_{out} for the out-of-band image rejection objective.		
	For each training tone at frequency f_k		
		perform time-aligned captures at the outputs of each of the I and Q ADCs	
		compare the Q capture data to the I capture data via cross-correlations or other means to estimate the mismatch response $H_k = H_\Delta(f_k) = H_q(f_k)/H_i(f_k)$	
		if f_k falls within the blocker band	
			assign this training point a weight of $\lambda_k = \lambda_{out}$
		else	
			assign this training point a weight of $\lambda_k = \lambda_{in}$
		end	
	end		
	Perform some form of weighted regression to solve for filter coefficients that minimize I/Q mismatch given f_k, λ_k, H_k for $k = 1, \ldots, K$.		

Measured Quadrature Sampling Image Rejection Results

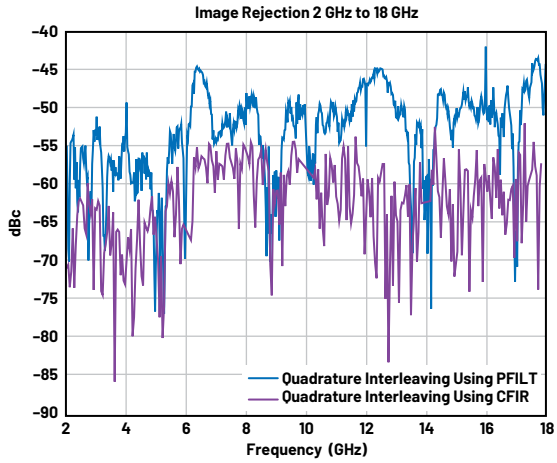

Figure 12. Measured direct quadrature sampling image rejection from 2 GHz to 18 GHz. Both QEC options of either the PFILT or CFIR are shown. The CFIR correction method shows results better than 50 dBc. The PFIR correction is slightly degraded in this data set and will be described in the following sections.

Measured image rejection results are shown in Figure 12. Results for both the PFILT and CFIR corrections are shown. Using the CFIR correction, an image rejection of >50 dBc is obtained. The results using the PFILT are slightly degraded, and the root cause can be seen from the data shown in Figure 13. When evaluating the amplitude and phase mismatch before and after QEC, note that fairly gross errors are corrected, but a rapid ripple across frequency remains after correction.

The PFILT runs at the full sample rate, while the CFIR runs at the decimated reduced sample rate. Because the PFILT and CFIR have a similar number of taps, this means that the CFIR can correct errors over a longer time period than the PFILT. The final result is that the CFIR provides a better correction for the test setup in use. However, the ripple is currently limited by impedance mismatch between the hybrid coupler and the ADC inputs and the long transmission lines between them. Simulations show that the ripple mismatch can be improved when the hybrid coupler is mounted adjacent to the ADC inputs that minimize small differences in signal path lengths.

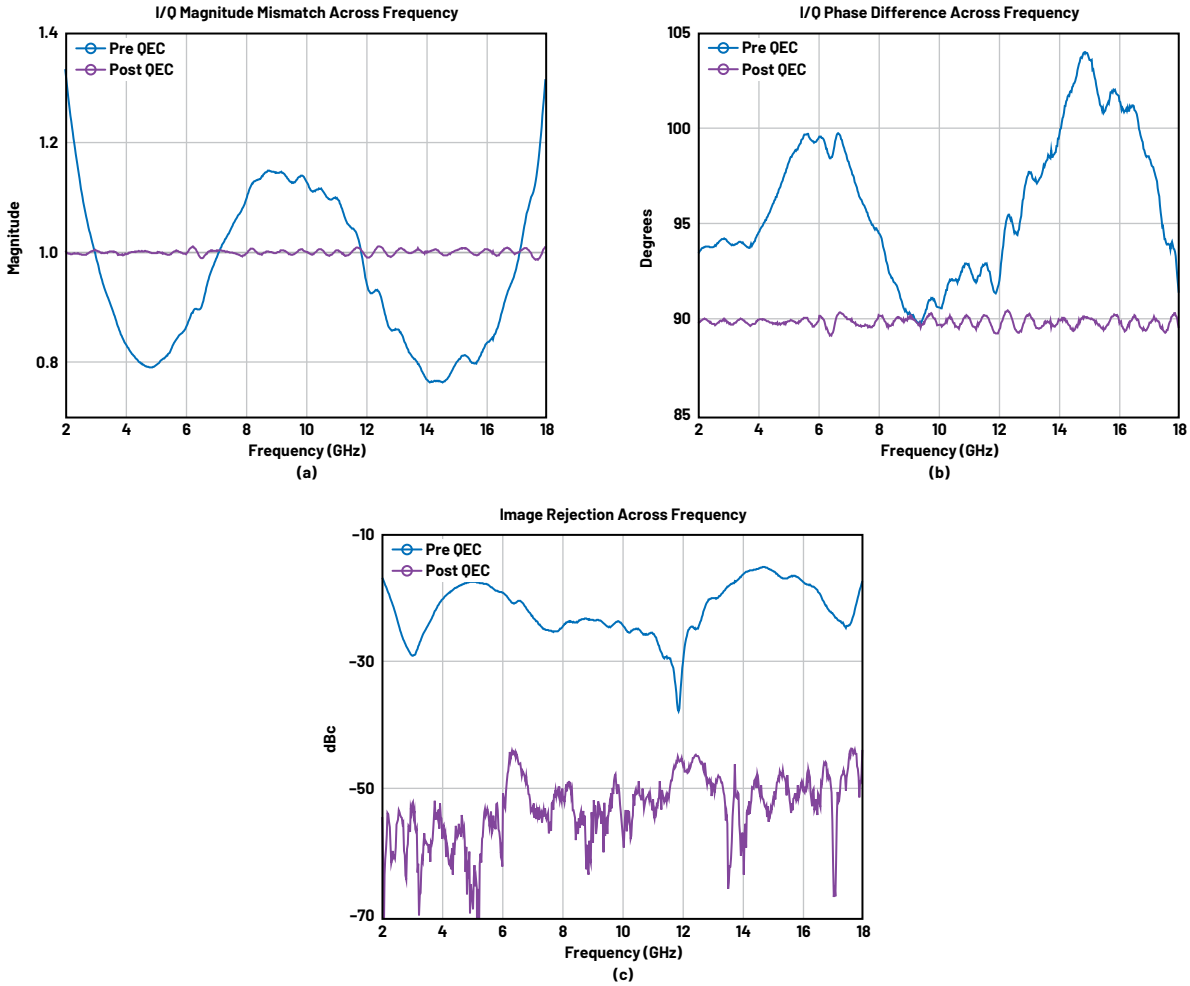

Figure 13. Amplitude mismatch, phase mismatch, and image rejection before and after QEC when using the PFILT QEC. The blue traces are before QEC. The purple traces are after QEC. The PFILT correction is limited to 16 taps at the full rate. With 16 taps, the correction is able to fix large errors that are slow moving with frequency, but the ripple that changes rapidly vs. frequency remains after the correction. The ripple is limited by the test configuration where impedance mismatch between the AD9084 and the quadrature hybrid reflects across relatively long transmission lines. An integrated board solution will mount the quadrature hybrid directly next to the device.

Conclusion

Direct quadrature sampling from 2 GHz to 18 GHz has been demonstrated. The following features enabled the result:

1. A wideband quadrature hybrid
2. ADCs with an input bandwidth through the second Nyquist zone
3. A method to ensure ADC data is time aligned
4. A QEC FIR filter at the full ADC rate
5. A complex DDC to reduce data rates
6. A quadrature correction algorithm that resolves input imbalance errors within the reduced data rate DDC output bandwidth

The solution cannot be achieved using only a single feature from this list. It is the combination of all of these features that creates the solution. Without any one of these, undesirable trade-offs may be required, or performance would be significantly reduced, rendering the solution unusable.

The approach presented provides a method to double the effective ADC sample rate without doubling digital data rates yet still maintaining embedded DSP functionality. These benefits create a method to trade off channel count vs. ADC rate at the application level without ADC modifications. Direct quadrature sampling or quadrature interleaving is not a replacement for time interleaving, but rather an alternative to consider among many, as software-defined radio systems continue to mature.

References

[1] Dave Frizelle and Frank Kearney. "Complex RF Mixers, Zero-IF Architecture, and Advanced Algorithms: The Black Magic in Next Generation SDR Transceivers." *Analog Dialogue*, Vol. 17, February 2017.

[2] Patrick Weirs. "Mirror, Mirror on the Wall—Understanding Image Rejection and Its Impact on Desired Signals." *Analog Dialogue*, Vol. 51, August 2017.

[3] Gabriele Manganaro and David H. Robertson. "Interleaving ADCs: Unraveling the Mysteries." *Analog Dialogue*, Vol. 49, July 2015.

About the Authors

Ian Beavers is a field applications engineer and customer labs manager for the Aerospace and Defense Systems team located at Analog Devices, Durham, North Carolina. He has worked for the company since 1999. Ian has over 25 years of experience in the semiconductor industry. Ian earned a bachelor's degree in electrical engineering from North Carolina State University and an M.B.A. degree from the University of North Carolina at Greensboro.

Peter Delos is a technical lead in the Aerospace and Defense Group at Analog Devices in Greensboro, North Carolina. He received his B.S.E.E. degree from Virginia Tech in 1990 and M.S.E.E. degree from NJIT in 2004. Peter has over 30 years of industry experience. Most of his career has been spent designing advanced RF/analog systems at the architecture level, PWB level, and IC level. He is currently focused on miniaturizing high performance receiver, waveform generator, and synthesizer designs for phased array applications.

Brian Reggiannini is a senior principal engineer in system design. He has designed, implemented, and supported system-level calibrations for several generations of Analog Devices' wireless transceiver products. His technical interests include signal processing, machine learning, embedded systems, and systems involving digitally assisted analog components. Brian earned Sc.B., Sc.M., and Ph.D. degrees from Brown University in 2007, 2009, and 2012, respectively.

Connor Bryant is a system applications engineer at Analog Devices working in the Aerospace and Defense Business Unit in Durham, North Carolina. He joined ADI in 2023. He is currently focused on RF mixed-signal chain design and analysis. He received his B.S.E.E degree from NC State University in 2022 and his M.S.E.E degree from NC State University in 2023.